Author:	Chen, Weijian ; Mao, Wenxin; Bach, Udo; Jia, Baohua; Wen, Xiaoming
Title:	Tracking dynamic phase segregation in mixed-halide perovskite single crystals under two-photon scanning laser illumination
Article number:	1900273
Year:	2019
Journal:	Small Methods
Volume:	3
Issue:	11
URL:	http://hdl.handle.net/1959.3/449781
Copyright:	Copyright © 2019 WILEY-VCH Verlag GmbH & Co. KGaA, Weinheim. This is the peer reviewed version of the following article: Chen, W., Mao, W., Bach, U., Jia, B., Wen, X., Tracking Dynamic Phase Segregation in Mixed-Halide Perovskite Single Crystals under Two-Photon Scanning Laser Illumination. Small Methods 2019, 3, 1900273, which has been published in final form at https://doi.org/10.1002/smtd.201900273. This article may be used for non-commercial purposes in accordance with Wiley Terms and Conditions for Use of Self-Archived Versions.

The definitive version is available at: https://doi.org/10.1002/smtd.201900273

Tracking Dynamic Phase Segregation in Mixed-Halide Perovskite Single Crystals under Two-photon Scanning Laser Illumination

Weijian Chen,[†] Wenxin Mao,[†] Udo Bach, Baohua Jia*, Xiaoming Wen*

Dr. W.Chen,[†] Prof. B.Jia,* Dr. X.Wen*
Centre for Translational Atomaterials,
Swinburne University of Technology,
Hawthorn 3122, VIC
Australia
Email: bjia@swin.edu.au, xwen@swin.edu.au

Dr. W.Mao,[†] Prof. U.Bach
Department of Chemical Engineering,
Monash University,
Clayton 3800 VIC,
Australia

Dr. W.Mao,[†] Prof. U.Bach
Centre of Excellence for Exciton Science,
Australian Research Council

[†] These authors contributed equally to this work

Keywords: perovskites, single crystal, phase segregation, two-photon, surface states

ABSTRACT

Photoinduced phase segregation in mixed halide perovskites has received considerable attention due to its critical roles in diminishing device performance in photovoltaic and light-emitting applications. Here we investigate dynamic photoinduced phase segregation and dark recovery in mixed halide perovskite single crystal microplatelets, combining depth-resolved, temporal-resolved and detection-wavelength selective spectroscopic imaging techniques. Under identical illumination, the edges and interior of microplatelets exhibit significantly different phase segregation. An intimate correlation of PL dynamics between I-phase and Br-phase indicates that the halide substitution is the dominant effect. In the dark, the phase-segregated crystals reversibly recover to the stable equivalence. This work clarifies the critical role of the edge state of the microplatelets and reveil the physical mechanism of phase segregation in mixed halide perovskites, which is of crucial importance for their applications in photovoltaics and photonics.

Metal-halide perovskites ($APbX_3$) have achieved significant progress in a wide range of optoelectronic applications, including light-emitting devices (LED)[1,2], photodetectors[3], lasing structure[4], and most importantly solar cells with power conversion efficiency exceeding 24.2%.[5–7] Optoelectronic properties of perovskites, including large absorption coefficient, long diffusion length, long carrier lifetimes and high tolerance of defects, have been confirmed to influence halide-based perovskite devices performance.[8–11] Since perovskite is a mixed carrier-ionic conductor, perovskite-based devices are significantly affected by the dynamics of mobile ions.[12–21] Mixed-halide perovskites with tunable bandgaps enable bandgap engineering in tandem solar cells and multiple-color LED.[22] However, mixed halide perovskites suffer from phase segregation when irradiated by visible light,[23] which is recently proved to be mediated by mobile ion diffusion.[24] Recently observed phase segregation in single crystal perovskite indicates that light-induced phase segregation is an intrinsic process in mixed halide perovskite.[25,26] The interfaces, including grain boundaries, crystal surfaces and edges, are suspected of fostering ion migration and phase segregation.[27,28] However, the dynamic processes of phase segregation are not fully understood. Visualization of phase segregation between grains and grain boundaries in polycrystalline perovskite films via optical microscope is very challenging, as grain sizes (usually 500 nm to 1000 nm) are close to the resolution limit of optical microscopes.[29] What is more, high surface defects density of polycrystalline perovskite films, especially at the grain boundaries,[28] greatly affect the observation of the intrinsic properties. Mixed halide perovskite single crystals are free of grain boundary and have much lower defect density,[30] therefore, more suitable for this study.

In recent reports of light-induced instabilities in mixed halide perovskites under widefield illumination,[24,26,31,32] light illumination is absorbed in the surface area due to the short penetration depth of bias light, which means that the interplay between surface states and crystal bulk states in light-induced phase segregations are still in lack. Besides, difficulties in analyzing the experimental results arise when the samples are simultaneously impacted by focused probing laser beams, wide field bias light, electron beams and/or electric field. Photo-induced phase segregation in single crystals is very quick (within 5s of widefield illumination),[25,26] while the influencing factors are intertwined. Therefore, it is difficult to disentangle the triggering, evolution, and recovery process of reversible photoinduced phase segregation. High-resolution characterization methods with fast response rate are required to disengage the structural interactions at play in single crystal perovskite under an only external bias. Two-photon absorption (TPA) is a third-order nonlinear optical process in which two low-energy photons are simultaneously absorbed if the temporal photon density is higher than the threshold.[33] Compared to one-photon absorption which occurs mainly at the surface area, TPA can be focused into bulk. Therefore, TPA based confocal microscopy is ideal to study the impact of bulk states in mixed halide perovskite during light illumination.[34–37]

Herein, we characterized dynamic photoinduced phase segregation and dark recovery in mixed halide $MAPbBr_xI_{3-x}$ perovskite single crystal microplatelets, combining depth-resolved, temporal-resolved and detection-wavelength selective spectroscopic imaging techniques. A significant difference in spatial distribution is presented between Br-phase and I-phase PL, where iodide substitution occurs preferably at the microplatelets edge. The comparison between one-photon and two-photon PL mapping provides clear evidence that surface and edge states play an important role in altering phase segregation. Two simultaneous processes during illumination, light-induced phase segregation and PL quenching, are separated according to their intrinsic physical mechanisms. The corresponding time constants are extracted from the illumination power dependent measurements, which exhibits a correlation between I-phase and Br-phase PL variation during illumination. These results are further confirmed by the dynamic recovery of these phase-segregated crystals in the dark.

$MAPbBr_xI_{3-x}$ perovskite single crystal microplatelets used in this study are fabricated using a solution-processed method, as previously reported.[26,38] Fabrication methods, Scanning electron microscope (SEM) and Energy-dispersive X-ray spectroscopy (EDS) images are provided in Supporting Information (SI). The I:Br ratio of these $MAPbBr_xI_{3-x}$ crystals is around 2:8 according to the UV-vis absorption spectra (Figure S2).[26] The XRD data of $MAPbBr_xI_{3-x}$ (Figure S3) shows there are no secondary phases. **Figure 1**a is the steady-state PL spectra of the $MAPbBr_xI_{3-x}$ microplatelets before and after probing laser scanning (488nm at 200 mW/cm^2) via a confocal laser scanning microscope. The light path of the microscope is shown in Figure S1, and other laser set-up details [39] are also provided in Experimental Section of SI. The pristine PL of microplatelets peaks at 550 nm. With continuous scanning laser excitation (90s) without any other bias light, an I-phase emission at 670 nm emerges, indicating phase segregation occurred. Note that the 488 nm pulsed laser is used as a probe source to scan the sample: with a short dwelling time at each pixel (1 ms) and each scan period of 10s, it was usually considered to have a negligible illumination effect in polycrystalline perovskite thin films.[29] However, significant phase segregation is observed in our monocrystalline $MAPbBr_xI_{3-x}$ microplatelets; this suggests that fast laser scanning is sufficient to induce phase segregation in such $MAPbBr_xI_{3-x}$ microplatelets. Fortunately, the fast system response of the confocal laser scanning microscope allows us to monitor the dynamic phase segregation process. Previous reports confirmed that the PL spectra exhibit significant wavelength shift from pure bromide phase at ~530 nm to the pure iodide phase at ~800 nm.[40] Hereafter we define the phase with PL wavelength between 530 nm and 580 nm as "Bromide-enriched emission phase" and the range between 620 nm and 720 nm as "Iodine-enriched emission phase", denoted as "Br-phase" and "I-phase", respectively. **Figure 1**b shows the time traces of both Br-phase and I-phase PL intensities during laser illumination. The corresponding two-dimensional PL mapping of the microplatelet are shown in **Figure 1**c-f. During continuous laser scanning time (0-630 s), I-phase PL continues to increase while Br-phase PL shows an initial decrease and then stabilizes at a lower intensity. Redshifted I-phase PL has an enhanced PL intensity at the edges of the microplatelets (**Figure 1**c-f), while pristine Br-phase PL has a distribution across the whole mircroplatelets. Once the laser is turned off and the sample is placed in the dark, I-phase PL quickly diminishes while Br-phase PL promptly recovers to its initial intensity within 200s. Note that the relatively weaker Br-phase PL at the center of the platelets is not ascribed to phase segregation, because its Br-phase PL exhibits the same variation and keeps relatively weaker than that in the other area of the microplatelet. Instead, it is reasonable to ascribe the relatively weak Br-phase PL to defects during crystal growth, which leads to relatively lower quantum efficiency in the pristine condition.

The phase segregation observed in single crystal perovskite proves that grain boundaries are not essential for phase segregation. However, the spatial contrast between the Br-phase and I-phase PL is intricate. Br-phase PL is distributed across the microplatelet area where I-phase PL tends to exhibit an enhanced intensity at the edges of the microplatelets. Essentially, at the identical excitation, the density of fluorophores together with the emission quantum yield determines the integrated PL intensity and thus determines the brightness of the PL mapping in each point. To clarify the origin for such an observation, the element distribution has been carefully measured by EDS. These EDS measurements have consistently shown that Br and I uniformly distributed across the microplatelets (Figure S4, SI). Therefore, the possibility of inhomogeneous element distribution can be safely excluded. Previous reports speculated that it might be owing to photonic waveguide mode.[25,41] We emphasize that PL imaging in this study is acquired based on a confocal scanning microscope in which each PL signal is collected from the excitation point; therefore, waveguided light is not prominent. It is speculated that the formation of I-phase at the edge is favorable to minimize the total strain energy of the perovskite microplatelets under continuous illumination.[25,42–44]

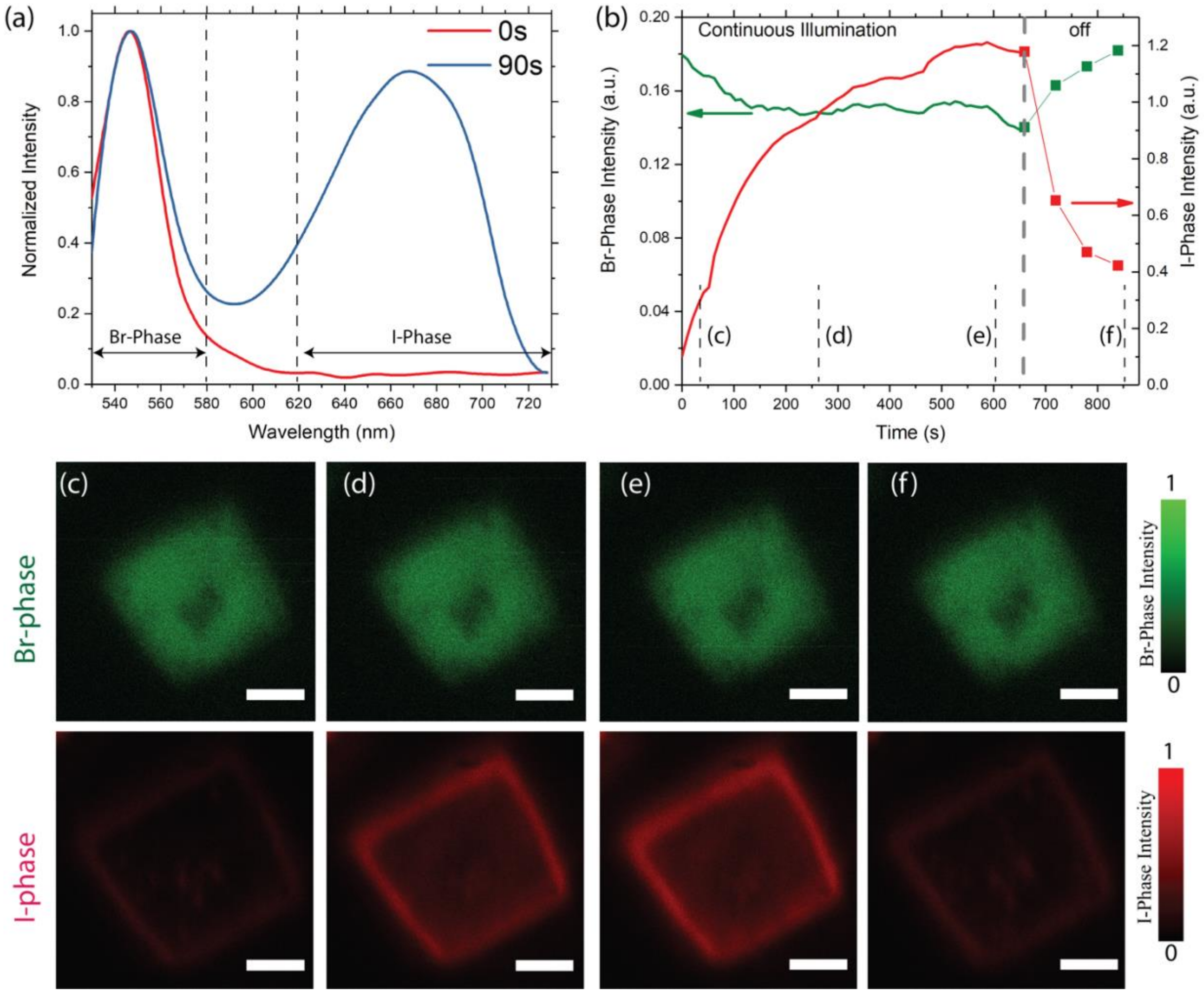

Figure 1. (a) Normalized PL spectra of the perovskite in pristine condition and after 90s of continuous laser scanning excitation; (b) PL intensities of Br-phase (530nm-580nm) and I-phase (620nm-720nm) as a function of time (0-630 s: continuous laser scaning; 630-850 s: recovery in the dark); (c-f) Br-phase PL and I-phase two-dimensional PL mapping at different time intervals marked in (b). All scale bars are 10 μm.

Please note that under one-photon excitation (488 nm) in **Figure 1**, the penetration depth of the incident laser is within the first 100 nm,[45] where the carrier dynamics are highly impacted by the surface state of the perovskite nanoplatelets. To investigate the impacts of surface state on photo-induced phase segregation, we conducted a comparison of one-photon and two-photon PL of the same microplatelet, as shown in **Figure 2**. The time to capture one two-dimensional PL mapping in **Figure 2** is 5s. As illustrated in **Figure 2a**, in one-photon case, PL originates from the vicinity of perovskite surface with a minor contribution from the bulk, while two-photon excitation is rooted into the perovskite, which allows observation of bulk effects. Phase segregation in the crystal bulk is induced by a 900 nm focused femtosecond pulsed laser beam (**Figure 2**b). The excitation power of both one- and two-photon excitation is calibrated to generate the same PL intensity to ensure the photogenerated carrier densities are comparable. For both excitation methods (**Figure 2**c&d), Br-phase PL distributes across the whole microplatelets and I-phase PL appears mainly at the edges of the microplatelet. However, there are a number of important differences between phase segregation by one-photon (**Figure 2**c) and two-photon (**Figure 2**d-f) excitation. The striking differences of the two-photon case emerge in the consecutive images (**Figure 2**e-f): I-phase PL appears at the crystal edge and followed by gradually migrating to the interior of the microplatelet, accompanied by the dramatic intensity drop of Br-phase PL at the same positions. The substitution of Br-phase PL by I-phase PL suggests that direct I-Br substitution, rather than a change of quantum efficiency, is the dominant effect in photo-induced phase segregation. It is worth noting that the positions where these I-phase fluorophores emerge are not stochastically distributed as previously reported by Bischak et al,[25] but firstly occupy the proximity of the edges (**Figure 2**e) and gradually flood into the crystal interior (**Figure 2**f). The corners of the platelets, where two edges are joining, is the most favorable area for phase segregation, which indicates that edges states are promoting phase segregation in mixed halide single crystals perovskite. One might suggest that the thickness of the microplatelets might affect the phase segregation and be revealed by two-photon excitation experiments, which has been discussed in Note 1 of SI.

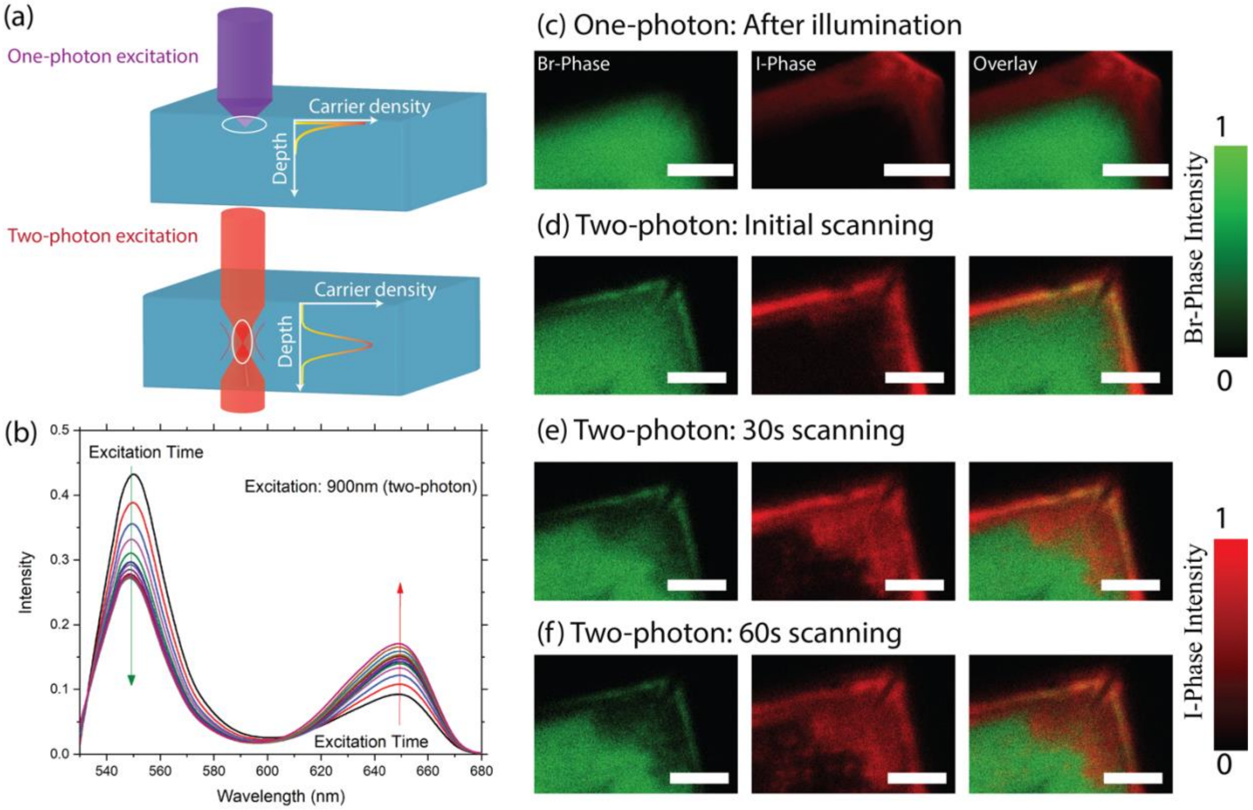

Figure 2. (a) Schematic of one-photon *versus* two-photon microscopy; (b) PL spectra of the perovskite continuously excited by a scanning laser in two-photon microscopy; two-dimensional PL mapping of Br-phase, I-phase and Phases-overlay excited by (c) one-photon absorption at 488nm and (d-f) two-photon absorption at 900nm. (d), (e) & (f) are sequence two-dimensional PL mapping under consecutive two-photon excitation.

Intensity and duration of illumination are the critical factors to induce phase segregation of mixed halide perovskite.[24,43,46] Herein we performed power dependent measurement on the perovskite microplatelets (200 to 800 mW/cm^2), as shown in **Figure 3**a. Similar to **Figure 1**, at low excitation power density, I-phase PL (Br-phase PL) quickly increases (decreases) within the first 100s and then stabilizes after longer excitation time. At higher power densities (400 mW/cm^2 and 800 mW/cm^2), I-phase PL exhibits an initial rapid increase, followed by the slow decline at the delayed time stage before stabilization. In contrast, Br-phase PL continues to decrease. Laser scanning illumination not only induces phase segregation but also results in PL quenching because of illumination activated mobile ions.[47] The simultaneous impacts of PL enhancement and quenching result in a complicated PL time trace.

To quantitatively analyze the dynamic phase segregation, we propose a model of PL quenching and enhancement to analyze the PL time traces under continuous illumination. Phase segregation is described by a saturation growth (quenching) process which increases (decreases) PL intensity for I-phase (Br-phase) PL. Illumination-induced PL quenching is fitted by an exponential decay model.[47] The I-phase and Br-phase PL time traces during continuous illumination are described as:

$$I_{\mathrm{I-Phase}}(t) = A_{\mathrm{sat}}^{\mathrm{I}} * \frac{t}{1+t/\tau_{\mathrm{sat}}^{\mathrm{I}}} - A_{\mathrm{exp}}^{\mathrm{I}} * (1 - \exp(t/\tau_{\mathrm{exp}}^{\mathrm{Br}}))) \qquad (1)$$

$$I_{\mathrm{Br-Phase}}(t) = I_{\mathrm{Br}}(0) - \mathrm{A}_{\mathrm{sat}}^{\mathrm{Br}} * \frac{t}{1+t/\tau_{\mathrm{sat}}^{\mathrm{Br}}} - \mathrm{A}_{\mathrm{exp}}^{\mathrm{Br}} * (1 - \exp(t/\tau_{\mathrm{exp}}^{\mathrm{Br}}))) \qquad (2)$$

where $\tau_{\mathrm{sat}}^{\mathrm{I}}$, $\tau_{\mathrm{exp}}^{\mathrm{I}}$, $\tau_{\mathrm{sat}}^{\mathrm{Br}}$ and $\tau_{\mathrm{exp}}^{\mathrm{Br}}$ are the time constants, $I_{\mathrm{Br}}(0)$ is the pristine Br-phase PL intensity, $A_{\mathrm{sat}}^{\mathrm{I}}$, $\mathrm{A}_{\mathrm{sat}}^{\mathrm{Br}}$, $A_{\mathrm{exp}}^{\mathrm{I}}$ and $\mathrm{A}_{\mathrm{exp}}^{\mathrm{Br}}$ are the corresponding weight ratios. In Equation (1), the first term (saturation growth function) describes the enhancement of I-phase PL due to halide substitution and the second part (exponential quenching function) describes PL quenching by light-activated mobile ions.[47,48] The fitted curves of Br-phase and I-phase PL time traces at 400 mw/cm^2 are shown in **Figure 3**b, with the curves of saturation and quenching components separately plotted in **Figure 3**c and **Figure 3**d. The time constants of both Br-phase PL saturation ($\tau_{\mathrm{sat}}^{\mathrm{Br}}$, 212.78s) and exponential component ($\tau_{\mathrm{exp}}^{\mathrm{Br}}$, 436.95s) are extremely close to those of I-phase PL ($\tau_{\mathrm{sat}}^{\mathrm{I}}$, 215.42s and $\tau_{\text{exp}}^{\text{I}}$, 446.21s), which exhibits an obvious correlation between Br-phase PL decrease and I-phase PL increase. For the purpose of confirming the correlation under different excitation power, we performed power dependent analysis, shown in Figure S5 (SI), which also present a correlation between Br-phase PL and I-phase PL time constants. Such correlation indicates that both phases are simultaneously influenced by the same process of phase segregation and PL quenching during illumination.

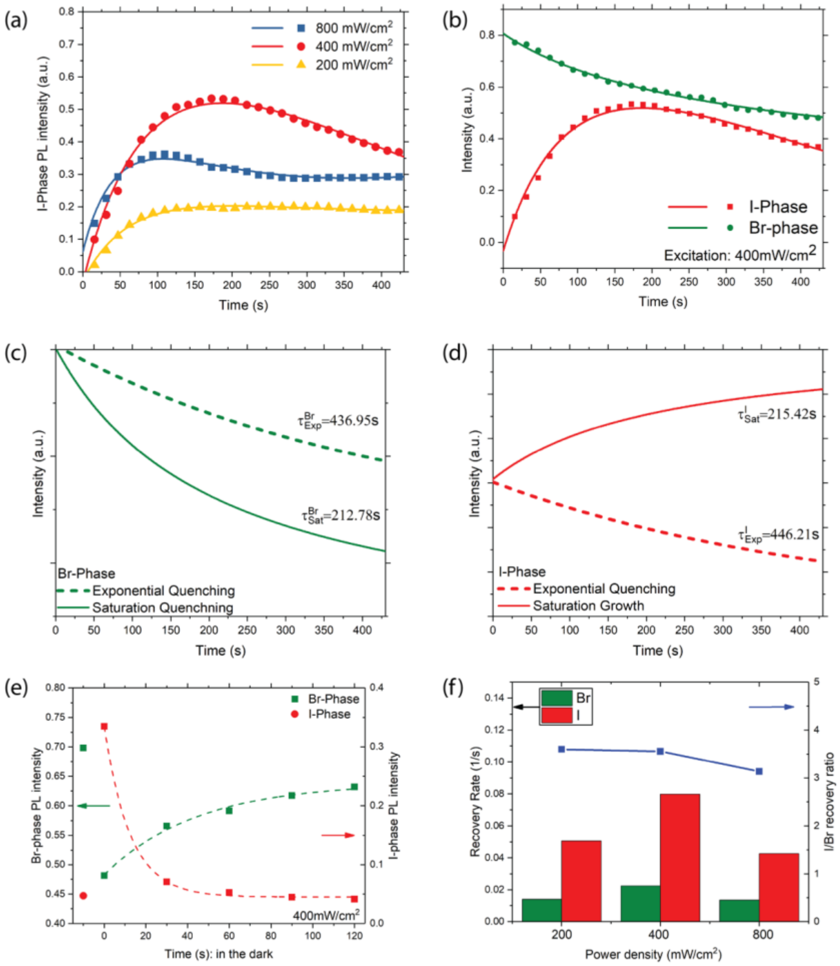

Figure 3. (1) Illumination power dependent I-phase PL intensity time traces (from 200 to 800 mW/cm^2); (b) PL intensity time traces of I-phase and Br-phase at 400 mW/cm^2; Separated PL curves of growth and quenching components of (c) Br-phase & (d) I-phase PL; (e) Br-phase and I-phase PL intensity *verse* time in the dark after illumination (400 mW/cm^2) with the intensity before time zero represents the pristine PL intensity; (f) Corresponding fitted recovery rate at different power density.

Figure 3e shows the recovery process in the dark after the continuous laser scanning at 400 mW/cm^2 (**Figure 3**a). Similar recovery processes at 200 mW/cm^2 and 800 mW/cm^2 in the dark are shown in Figure S6 (SI). Recovery in the dark is a much faster process in single crystals (within hundreds of seconds) compared to that in polycrystalline films (40-60 minutes).[49] The recovery dynamics of both I-phase and Br-phase PL are fitted by a single-exponential function: $I(t) = I_0 + A\exp(t/\tau)$, and the recovery constant is defined as $C_{re} = 1/\tau$, plotted in **Figure 3**f. It is worth noting that I-phase PL recovery is much faster than Br-phase PL recovery. The ratio between I-phase and Br-phase recovery constant is around 3.5, nearly independent on the illumination power density. Since Br-phase fluorophores are distributed with a much larger amount than I-phase fluorophores, the recovery of Br-phase PL is not as significant as the quenching of I-phase PL. It is reasonable to speculate that the fast I-phase PL decrease is due to "I-to-Br" substitution, as Pb^{2+}/Br^- binding is more favorable than Pb^{2+}/I^- binding in mixed halide perovskite binding formation.[31] I-phase fluorophores diminish once I^- ions in the lattices is substituted, followed by the formation of Br-phase fluorophores. Therefore, Br-phase PL recovery is at a slow constant rate.

Based on the above experimental results, we propose a mechanism, as schematically shown in **Figure 4**, to interpret the different phase segregations occurring in the edge and interior of a mixed-halide perovskite single crystal: charge carriers are photogenerated during illumination, followed by recombination, diffusion and surface trapping. It has been showed that charge carrier diffusion length exceeds 175 μm in the perovskite single crystal,[50] photogenerated charge carriers diffuse for a long distance before trapped by defects or radiatively recombined. Taking into account the long diffusion length and low defect trapping in single crystal perovskite, it is expected that significantly higher density of charge carriers is presented at the edges, as the crystal edges serve as a dam of diffusing carriers under continuous illumination. Excessive charge carriers at the edges result in a higher density of phonons[43] and higher potential energy in the lattices.[51] Therefore, it is expected to have a higher possibility to activate the halide ions from lattice into interstitials and vacancies. These activated interstitials and vacancies intermediately assist the phase segregation by halide substitution:[31]

$$\mathrm{I_{in}^{-}} + \mathrm{MAPbBr_{x}I_{3-x}} \xrightarrow[\mathrm{Vacancies}]{h\nu \rightarrow \mathrm{e^{-}}\,\&\,\mathrm{h^{+}}} \mathrm{Br_{in}^{-}} + \mathrm{MAPbBr_{x-y}I_{3-x+y}} \qquad (3)$$

It has been reported that in continuous wide field light soaking condition, phase segregation in the interior of the microplatelets appears with longer illumination time. However, only minor I-phase PL has been observed in the microplatelets interior via one-photon laser scanning illumination in our confocal microscopes. The photo-generated charge carriers are predominantly distributed at the top surface area due to the short penetration depth of the 488 nm laser beam (100 nm). As shown in **Figure 4**a, a large number of charge carriers are trapped by the non-radiative defects at the top surface before arriving at the edges. A lower carrier density is presented in the interiors than the edges. Therefore, I-phase PL can only be observed at the edges in one-photon laser scanning illumination. In two-photon laser scanning illumination (**Figure 4**b), the photogenerated charge carriers distribute dominantly at the excitation volume deep in the crystal bulk. Therefore, photogenerated charge carriers are less likely to be trapped by surface defects and more easily diffuse to the edges. As charge carriers efficiently accumulate at the crystal edges (mobile ion activated), I-phase fluorophores is firstly observed at the edges and later propagate into the microplatelets interior. During recovery in the dark, no charge carriers to continuously activate mobile ion. Excessive Br^{-} ions tend to substitute the I^{-} ions in the perovskite lattice, as Pb^{2+}/Br^{-} binding is more favorable in mixed halide perovskite binding formation.[31] Therefore, Br-phase PL promptly recovers, while I-phase PL quickly diminishes.

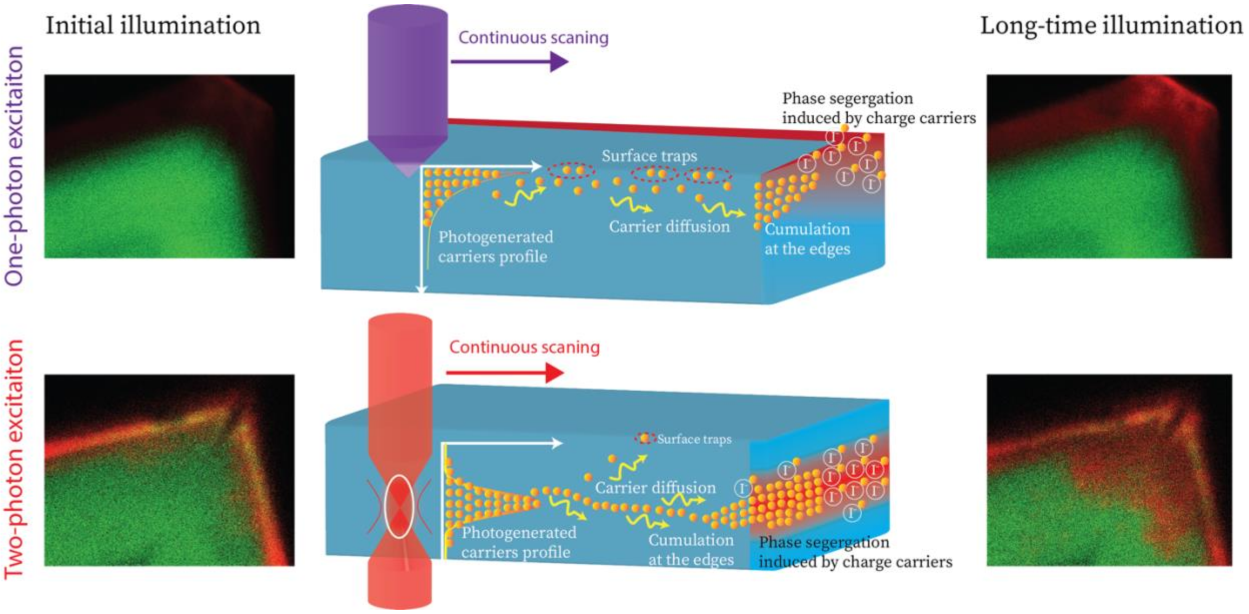

Figure 4. Schematic of the carrier transports and photo-induced phase segregation process under one-photon and two-photon illumination.

In summary, we have studied the dynamic photo-induced phase segregation in mixed halide perovskite single crystals, and the dark recovery process using one- and two-photon confocal microscope. Pristine Br-phase PL is distributed across the sample interior while phase-shifted I-phase PL is preferably enhanced at the edges of microplatelets. We confirm the edge/surface states play a critical role in altering the phase segregation. By modelling the PL dynamic variation, taking phase segregation and halide substitution into account, as well as simultaneous PL quenching due to ion activation, we fully separate the PL time trace under continuous illumination. We show that there is an obvious PL correlation between I-phase and Br-phase during illumination, where the halide substitution is the dominant effect. Light-activated mobile ions not only facilitate the phase segregation but also accelerate non-radiative recombination. By placing the exposed sample in the dark, phase-segregated perovskite reversibly recovers. A model of activated-vacancy assisted phase segregation, altered by surface and edges states, is proposed to describe the photoinduced process in the mixed halide monocrystalline perovskite. This work provides a new insight of phase segregation in single crystal mixed halide perovskite and is useful for applications in photovoltaics and photonics.

Supporting Information

Supporting Information is available from the Wiley Online Library or from the author. Experimental methods and set up, SEM, and EDS, PL time traces at various power density.

Notes

The authors declare no competing financial interest.

Acknowledgements

W.C. and M.W. contributed equally to this work. B.J. acknowledges support from the Australia Research Council through the Discovery Project scheme (DP150102972, DP190103186).

References

[1] M. Yuan, L. N. Quan, R. Comin, G. Walters, R. Sabatini, O. Voznyy, S. Hoogland, Y. Zhao, E. M. Beauregard, P. Kanjanaboos, Z. Lu, D. H. Kim, E. H. Sargent, *Nat. Nanotechnol.* **2016**, *11*, 1.

[2] H. Cho, S. H. Jeong, M. H. Park, Y. H. Kim, C. Wolf, C. L. Lee, J. H. Heo, A. Sadhanala, N. S. Myoung, S. Yoo, S. H. Im, R. H. Friend, T. W. Lee, *Science (80-.).* **2015**, *350*, 1222.

[3] M. Ahmadi, T. Wu, B. Hu, *Adv. Mater.* **2017**, *29*, 1605242.

[4] G. Xing, N. Mathews, S. S. Lim, N. Yantara, X. Liu, D. Sabba, M. Grätzel, S. Mhaisalkar, T. C. Sum, *Nat. Mater.* **2014**, *13*, 476.

[5] M. A. Green, Y. Hishikawa, E. D. Dunlop, D. H. Levi, J. Hohl-Ebinger, A. W. Y. Ho-Baillie, *Prog. Photovoltaics Res. Appl.* **2018**, *26*, 3.

[6] NREL, "NREL. Efficiency Chart.," can be found under https://www.nrel.gov/pv/assets/pdfs/best-research-cell-efficiencies-190416.pdf, **2019**.

[7] F. Zheng, W. Chen, T. Bu, K. P. Ghiggino, F. Huang, Y. Cheng, P. Tapping, T. W. Kee, B. Jia, X. Wen, *Adv. Energy Mater.* **2019**, 1901016.

[8] Q. Dong, Y. Fang, Y. Shao, P. Mulligan, J. Qiu, L. Cao, J. Huang, *Science (80-.).* **2015**,

347, 967.

[9] J. H. Noh, S. H. Im, J. H. Heo, T. N. Mandal, S. Il Seok, *Nano Lett.* **2013**, *13*, 1764.

[10] P. P. Boix, S. Agarwala, T. M. Koh, N. Mathews, S. G. Mhaisalkar, *J. Phys. Chem. Lett.* **2015**, *6*, 898.

[11] Z. Gan, X. Wen, W. Chen, C. Zhou, S. Yang, G. Cao, K. P. Ghiggino, H. Zhang, B. Jia, *Adv. Energy Mater.* **2019**, *1900185*, 1900185.

[12] C. Li, S. Tscheuschner, F. Paulus, P. E. Hopkinson, J. Kießling, A. Köhler, Y. Vaynzof, S. Huettner, *Adv. Mater.* **2016**, *28*, 2446.

[13] P. Calado, A. M. Telford, D. Bryant, X. Li, J. Nelson, B. C. O'Regan, P. R. F. Barnes, *Nat. Commun.* **2016**, *7*, 13831.

[14] J. M. Azpiroz, E. Mosconi, J. Bisquert, F. De Angelis, *Energy Environ. Sci.* **2015**, *8*, 2118.

[15] Z. Xiao, Y. Yuan, Y. Shao, Q. Wang, Q. Dong, C. Bi, P. Sharma, A. Gruverman, J. Huang, *Nat. Mater.* **2015**, *14*, 193.

[16] G. Y. Kim, A. Senocrate, T. Y. Yang, G. Gregori, M. Grätzel, J. Maier, *Nat. Mater.* **2018**, *17*, 445.

[17] D. Li, H. Wu, H.-C. Cheng, G. Wang, Y. Huang, X. Duan, *ACS Nano* **2016**, *10*, 6933.

[18] X. Guan, W. Hu, M. A. Haque, N. Wei, Z. Liu, A. Chen, T. Wu, *Adv. Funct. Mater.* **2018**, *28*, 1704665.

[19] Y. Yuan, J. Huang, *Acc. Chem. Res.* **2016**, *49*, 286.

[20] W. Li, M. U. Rothmann, A. Liu, Z. Wang, Y. Zhang, A. R. Pascoe, J. Lu, L. Jiang, Y. Chen, F. Huang, Y. Peng, Q. Bao, J. Etheridge, U. Bach, Y.-B. B. Cheng, *Adv. Energy Mater.* **2017**, *1700946*, 1700946.

[21] A. Senocrate, I. Moudrakovski, G. Y. Kim, T.-Y. Yang, G. Gregori, M. Grätzel, J. Maier,

Angew. Chemie Int. Ed. **2017**, *56*, 7755.

[22] A. Sadhanala, F. Deschler, T. H. Thomas, S. E. Dutton, K. C. Goedel, F. C. Hanusch, M. L. Lai, U. Steiner, T. Bein, P. Docampo, D. Cahen, R. H. Friend, *J. Phys. Chem. Lett.* **2014**, *5*, 2501.

[23] E. T. Hoke, D. J. Slotcavage, E. R. Dohner, A. R. Bowring, H. I. Karunadasa, M. D. McGehee, *Chem. Sci.* **2015**, *6*, 613.

[24] M. C. Brennan, S. Draguta, P. V. Kamat, M. Kuno, *ACS Energy Lett.* **2018**, *3*, 204.

[25] C. G. Bischak, A. B. Wong, E. Lin, D. T. Limmer, P. Yang, N. S. Ginsberg, *J. Phys. Chem. Lett.* **2018**, *9*, 3998.

[26] W. Mao, C. R. Hall, A. S. R. Chesman, C. Forsyth, Y.-B. Cheng, N. W. Duffy, T. A. Smith, U. Bach, *Angew. Chemie Int. Ed.* **2019**, *58*, 2893.

[27] J. S. Yun, J. Seidel, J. Kim, A. M. Soufiani, S. Huang, J. Lau, N. J. Jeon, S. Il Seok, M. A. Green, A. Ho-Baillie, *Adv. Energy Mater.* **2016**, *6*, 1600330.

[28] W. Li, M. U. Rothmann, A. Liu, Z. Wang, Y. Zhang, A. R. Pascoe, J. Lu, L. Jiang, Y. Chen, F. Huang, Y. Peng, Q. Bao, J. Etheridge, U. Bach, Y.-B. Cheng, *Adv. Energy Mater.* **2017**, *1700946*, 1700946.

[29] S. Chen, X. Wen, J. S. Yun, S. Huang, M. Green, N. J. Jeon, W. S. Yang, J. H. Noh, J. Seo, S. Il Seok, A. Ho-Baillie, *ACS Appl. Mater. Interfaces* **2017**, *9*, 6072.

[30] D. Shi, V. Adinolfi, R. Comin, M. Yuan, E. Alarousu, A. Buin, Y. Chen, S. Hoogland, A. Rothenberger, K. Katsiev, Y. Losovyj, X. Zhang, P. A. Dowben, O. F. Mohammed, E. H. Sargent, O. M. Bakr, *Science (80-.).* **2015**, *347*, 519.

[31] S. J. Yoon, M. Kuno, P. V. Kamat, *ACS Energy Lett.* **2017**, *2*, 1507.

[32] D. J. Slotcavage, H. I. Karunadasa, M. D. McGehee, *ACS Energy Lett.* **2016**, *1*, 1199.

[33] M. Rumi, J. W. Perry, *Adv. Opt. Photonics* **2010**, *2*, 451.

[34] W. Chen, X. Wen, M. Latzel, M. Heilmann, J. Yang, X. Dai, S. Huang, S. Shrestha, R. Patterson, S. Christiansen, G. Conibeer, *ACS Appl. Mater. Interfaces* **2016**, *8*, 31887.

[35] S. Zou, G. Yang, T. Yang, D. Zhao, Z. Gan, W. Chen, H.-Z. Zhong, X. Wen, B. Jia, B. Zou, *J. Phys. Chem. Lett.* **2018**, *9*, 4878.

[36] X. Hu, X. Wang, P. Fan, Y. Li, X. Zhang, Q. Liu, W. Zheng, G. Xu, X. Wang, X. Zhu, A. Pan, *Nano Lett.* **2018**, *18*, 3024.

[37] X. Wang, H. Zhou, S. Yuan, W. Zheng, Y. Jiang, X. Zhuang, H. Liu, Q. Zhang, X. Zhu, X. Wang, A. Pan, *Nano Res.* **2017**, *10*, 3385.

[38] W. Mao, J. Zheng, Y. Zhang, A. S. R. Chesman, Q. Ou, J. Hicks, F. Li, Z. Wang, B. Graystone, T. D. M. Bell, M. U. Rothmann, N. W. Duffy, L. Spiccia, Y. B. Cheng, Q. Bao, U. Bach, *Angew. Chemie - Int. Ed.* **2017**, *56*, 12486.

[39] W. Chen, X. Wen, J. Yang, M. Latzel, R. Patterson, S. Huang, S. Shrestha, B. Jia, D. J. Moss, S. Christiansen, G. Conibeer, *Nanoscale* **2018**, *10*, 5358.

[40] G. E. Eperon, S. D. Stranks, C. Menelaou, M. B. Johnston, L. M. Herz, H. J. Snaith, *Energy Environ. Sci.* **2014**, *7*, DOI 10.1039/c3ee43822h.

[41] Q. Zhang, R. Su, X. Liu, J. Xing, T. C. Sum, Q. Xiong, *Adv. Funct. Mater.* **2016**, *26*, 6238.

[42] X. Tang, M. van den Berg, E. Gu, A. Horneber, G. J. Matt, A. Osvet, A. J. Meixner, D. Zhang, C. J. Brabec, *Nano Lett.* **2018**, *18*, 2172.

[43] C. G. Bischak, C. L. Hetherington, H. Wu, S. Aloni, D. F. Ogletree, D. T. Limmer, N. S. Ginsberg, *Nano Lett.* **2017**, *17*, 1028.

[44] H. Zhang, X. Fu, Y. Tang, H. Wang, C. Zhang, W. W. Yu, X. Wang, Y. Zhang, M. Xiao, *Nat. Commun.* **2019**, *10*, 1088.

[45] J. Yang, X. Wen, H. Xia, R. Sheng, Q. Ma, J. Kim, P. Tapping, T. Harada, T. W. Kee, F. Huang, Y.-B. Cheng, M. Green, A. Ho-Baillie, S. Huang, S. Shrestha, R. Patterson, G. Conibeer, *Nat. Commun.* **2017**, *8*, 14120.

[46] A. J. Barker, A. Sadhanala, F. Deschler, M. Gandini, S. P. Senanayak, P. M. Pearce, E. Mosconi, A. J. Pearson, Y. Wu, A. R. Srimath Kandada, T. Leijtens, F. De Angelis, S. E. Dutton, A. Petrozza, R. H. Friend, *ACS Energy Lett.* **2017**, *2*, 1416.

[47] S. Chen, X. Wen, S. Huang, F. Huang, Y. Cheng, M. Green, A. Ho-Baillie, *Sol. RRL* **2017**, *1*, 1600001.

[48] X. Deng, X. Wen, S. Huang, R. Sheng, T. Harada, T. W. Kee, M. Green, A. Ho-Baillie, *J. Phys. Chem. C* **2016**, *120*, 2542.

[49] S. J. Yoon, S. Draguta, J. S. Manser, O. Sharia, W. F. Schneider, M. Kuno, P. V. Kamat, *ACS Energy Lett.* **2016**, *1*, 290.

[50] Q. Dong, Y. Fang, Y. Shao, P. Mulligan, J. Qiu, L. Cao, J. Huang, *Science.* **2015**, *347*, 967.

[51] Y.-C. Zhao, W.-K. Zhou, X. Zhou, K.-H. Liu, D.-P. Yu, Q. Zhao, *Light Sci. Appl.* **2016**, *6*, e16243.